Journal of Materials Chemistry C

Accepted Manuscript

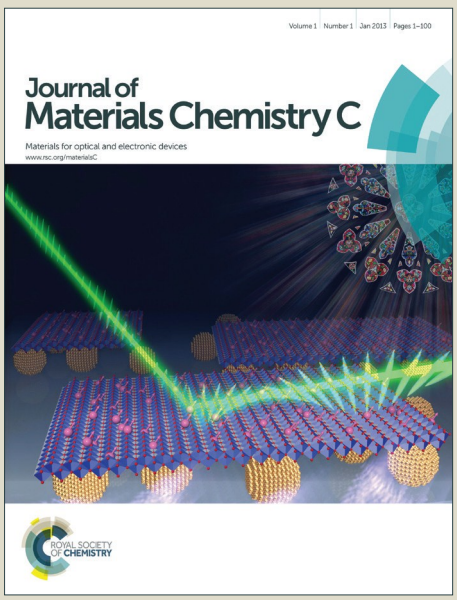

ROYAL SOCIETY OF CHEMISTRY

www.rsc.org/materialsC

Journal Name

RSCPublishing

ARTICLE

Solution-Processable Iridium Phosphors for Efficient Red and White Organic Light-Emitting Diodes with Low Roll-Off

Cite this: DOI: 10.1039/x0xx00000x

Received 00th January 2012,
Accepted 00th January 2012

DOI: 10.1039/x0xx00000x

www.rsc.org/

Ya-Li Deng, Lin-Song Cui, Yuan-Liu, Zhao-Kui Wang,* Zuo-Quan Jiang, and Liang-Sheng Liao*

A new red phosphorescent material Ir(dmppm)$_2$(dmd) which is a pyrimidine-based iridium (III) complex, has been synthesized and successfully used to fabricate solution-processed red and white organic light-emitting diodes (OLEDs). Due to its excellent solubility in common organic solvents and its good compatibility with the host material, a record current efficiency of 27.2 cd A^{-1} so far with satisfactory Commission International de l'Eclairage (CIE) coordinates of (0.60, 0.40) has been achieved for partially solution-processed red OLEDs by using Ir(dmppm)$_2$(dmd) as a dopant. Furthermore, the fabricated two-component "warm-white" OLEDs based on Ir(dmppm)$_2$(dmd) red emitter demonstrate a maximum current efficiency of 28.9 cd A^{-1}, which can meet the call for physiologically-friendly indoor illumination.

Introduction

White organic light-emitting diodes (OLEDs) are considered as the promising candidates for next-generation lighting applications.[1-4] For fluorescent materials, the internal quantum efficiency (IQE) is limited to 25% because of the non-radiative decay of the triplet excitons.[5] To achieve 100% of IQE, phosphorescent materials incorporating heavy metals into organic aromatic frameworks have been developed to facilitate the transition from the lowest triplet excited state (T_1) to the ground state (S_0).[6-9] Recently, thermally activated delayed fluorescent (TADF) materials such as cuprous complexes, zinc complexes and metal-free organic molecules are also developed for efficient blue and green OLEDs.[10-12] Comparison with the other two color emissions,[13-14] red light emission is still not satisfying with the device efficiency because the red TADF emitters show relatively low fluorescence quantum yields (Φ) and long TADF lifetime.[15] Fortunately, iridium complexes are promising red emitters owing to their high Φ and short emission lifetimes (τ_p).[16]

Generally, thermal evaporation technique is commonly utilized for depositing the OLED devices.[17-18] Different from thermal evaporation, solution processing is more promising and intriguing than vacuum deposition by its advantages of time saving, low energy-consumption, flexibility, and large-area possibility.[19-20] For example, Li et al. recently reported high performance solution-processed red OLEDs based on 2-phenylbenzothiazole with impressive maximum current efficiency of 14.49 cd A^{-1}.[21] However, the efficiency of solution-processed red OLEDs is still inferior to that of vacuum-deposited OLEDs and high performance solution-processed red OLEDs are rarely reported until now.[22-26]

According to our previous reports, pyrimidine-type ligand is an excellent building block with good thermal and morphological stability. With efforts, red phosphorescent OLEDs based on pyrimidine-based iridium (III) complexes demonstrated high EQE over 28%.[27-28] In this paper, we designed and synthesized another iridium (III) complex, Ir(dmppm)$_2$(dmd), by introducing a pyrimidine moiety as a cyclometalating ligand and a 2,5-dimethylhexane-3,4-dione (dmd) moiety as an ancillary ligand for red and white phosphorescent OLEDs. Solution-processable phosphorescent red OLEDs based on Ir(dmppm)$_2$(dmd) show impressive EL performance with stable red emission and high CE of 27.2 cd A^{-1} with CIE coordinates of (0.60, 0.40). Furthermore, a two-component "warm-white" PhOLED based on bis [3, 5-difluoro-2-(2-pyridyl) phenyl-(2-carboxypyridyl)]-iridium (FIrpic) and Ir(dmppm)$_2$(dmd) emitters approaches a maximum current efficiency of 28.9 cd A^{-1}. The solution-processable new phosphorescent material can be regarded as an excellent dopant for red and white PhOLEDs.

Results and discussions

Synthesis and Characterization

The synthetic routes and chemical structure of the iridium complex Ir(dmppm)$_2$(dmd) are shown in Scheme 1. The new iridium complex was facilely prepared through two-step sequence. First, iridium chloride trihydrate was reacted with excess of ligands to afford dichloride bridged iridium (III) dimers. Second, the dimers can be readily converted to the monomeric complex Ir(dmppm)$_2$(dmd) by replacing the bridging chlorides with 2,5-dimethylhexane-3,4-dione in the presence of sodium carbonate as base. The chemical structure of Ir(dmppm)$_2$(dmd) was fully characterized by ^{1}H NMR and ^{13}C NMR spectroscopies, mass spectrometry and elemental analysis. The detailed synthetic methods and analysis are described in the Experimental Section. And the PLQY of this complex is 0.88. The high photoluminescence quantum yield determined its relatively excellent device performance (EQE) even in the solution process.

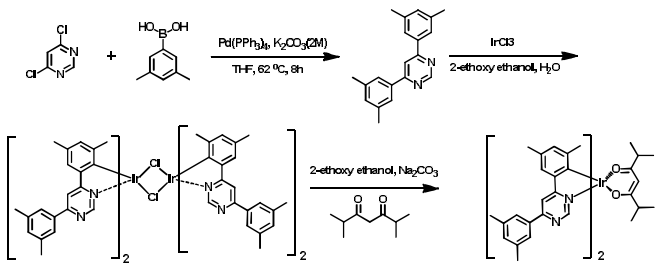

Scheme 1 Synthesis of ligands and iridium(III) complexes Ir(dmppm)$_2$(dmd).

Photophysical properties

Room-temperature UV-Vis absorption and fluorescence (PL) spectra of Ir(dmppm)$_2$(dmd) in CH_2Cl_2 solution and phosphorescence (Phos) spectra of the compound measured in a frozen 2-methyltetrahydrofuran matrix at 77 K are displayed in Fig.1. The strong absorption bands between 200 and 380 nm in the UV region with distinct vibronic features are assigned to the spin-allowed ligand-centered $^1\pi$-π* intraligand charge-transfer transitions in the complexes.[29] The bands extending into the visible region between 380 and 460 nm can be assigned to spin-allowed metal-to-ligand charge transfer (^{1}MLCT) mixed with an interligand charge transfer. However, the bands at the longer wavelength (> 460 nm) can be assigned to both spin–orbit coupling enhanced $^3\pi$-π* and ^{3}MLCT transition. These features indicate that the spin forbidden ^{3}MLCT gains intensity through mixing with the higher-lying ^{1}MLCT transition by the strong spin–orbit coupling on the iridium atom, which results in an strong absorption comparable to the allowed ^{1}MLCT. These features are analogous to other complexes with (C-N)$_2$Ir(acac) molecular formula as reported previously.[30] Upon photoexcitation at the absorption maximums, the complex in CH_2Cl_2 shows intense room-temperature phosphorescence with the orange major emission peaks at 604 nm in the PL spectra. The broad structureless spectral features of red emitter Ir(dmppm)$_2$(dmd) reveal that PL originates primarily from the ^{3}MLCT state. Compared with the emission spectra at ambient temperature, the phosphorescence spectra measured from a frozen 2-methyltetrahydrofuran matrix at 77 K shows apparent vibrational fine structure, indicating that the mixing between the ^{3}MLCT and $^3\pi$-π* levels is so effective that almost ligand-centered emission could be observed in the frozen matrix.[31]

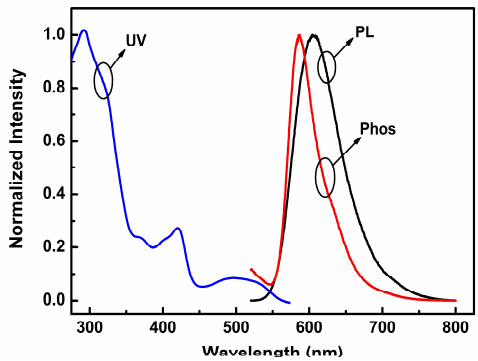

Fig. 1 Room-temperature UV-Vis absorption and photoluminescence (PL) spectrum of Ir(dmppm)$_2$(dmd) in CH_2Cl_2 solution and phosphorescence (Phos) spectrum of the compound measured in a frozen 2-methyltetrahydrofuran matrix at 77 K.

Electroluminescent properties

The electrochemical behaviors of Ir(dmppm)$_2$(dmd) was examined by cyclic voltammetry using ferrocene as the reference, and the results are shown in Fig.2. Upon anodic sweep in deoxygenated CH_2Cl_2, the complex exhibited a reversible oxidation wave with the oxidative potential at 0.83 V. The oxidation process is generally considered to be attributed to the metal-centered Ir^{III}/Ir^{IV} oxidation couple.[32] On the basis of the onset potentials of the oxidation, the HOMO energy level could be estimated from the onset of oxidation potentials relative to the vacuum level is -5.33 eV, which are almost consistent with the UPS measurement under vacuum (Supporting Information). The optical band gap (Eg) of Ir(dmppm)$_2$(dmd) is 2.05 eV, which is calculated from the thr-

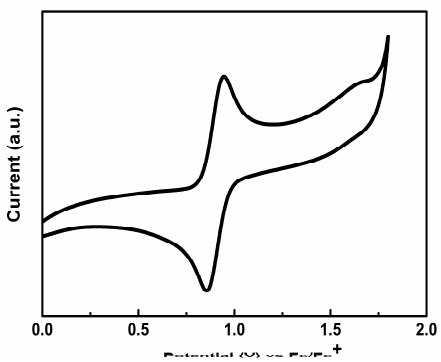

Fig. 2 Cyclic voltammogram of Ir(dmppm)$_2$(dmd) in dichloromethane solution for oxidation.

-eshold of the absorption spectra in CH_2Cl_2 solution. The LUMO level of Ir(dmppm)$_2$(dmd) is determined as -3.34 eV, which according to the equation $E_{LUMO} = E_{HOMO} + Eg$.[33] The results indicate that the generated excitons are able to be trapped on dopant in the doping system and lead to high device efficiency.

Solution processed red OLEDs

Ir(dmppm)$_2$(dmd) exhibits excellent solubility in chlorobenzene and good miscibility with the TCTA host. As shown in Fig. 3, the morphology images of spin-coated TCTA: Ir(dmppm)$_2$(dmd) film exhibits fairly smooth surface morphology with a smallest root-mean-square (RMS) surface roughness of 0.13 nm compared with the pure TCTA film with a roughness of 0.31 nm. Flatter surface morphology suggests smooth interface contacts between the emitting layer and the adjacent interfacial layers. Solution-processed OLED devices were fabricated with a configuration of ITO/PEDOT:PSS (40 nm)/TCTA: x wt% Ir(dmppm)$_2$(dmd) (45 nm)/TPBI (40 nm)/Liq(2nm)/Al (120 nm), to evaluate the electroluminescent properties of the new emissive phosphor of Ir(dmppm)$_2$(dmd). Where, poly(3,4-ethylenedioxythiophene): poly(styrenesulphonate) (PEDOT:PSS) was employed as hole-injecting layer (HIL), x is the doping concentration of Ir(dmppm)$_2$(dmd), 4,4',4''-tris(N-carbazolyl)-triphenylamine (TCTA) acted as the host material for its excellent film-forming property and hole-transporting characteristics, 1,3,5-tris(N-phenylbenzimidazol-2-yl)benzene (TPBI) was used as electron-transporting and hole-blocking layer, 8-hydroxyquinolinolato-lithium (Liq) served as the electron-injecting layer.

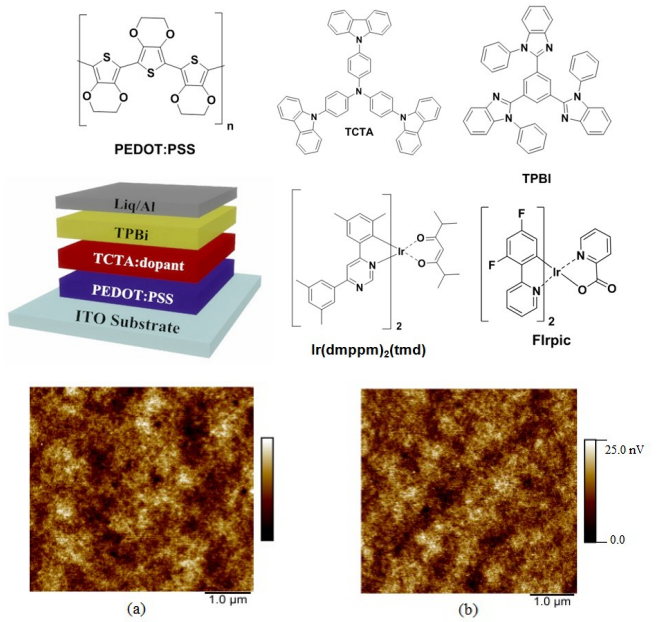

Fig. 3 The device architecture and the molecular structures used in the device and the morphology images of (a) TCTA and (b) TCTA: Ir(dmppm)$_2$(dmd) film measured by AFM.

The EL characteristics of the red OLEDs, including J-V-L curves, efficiency and EL spectra are displayed in Fig.4, and some key performance parameters of the red OLEDs are summarized in Table 1. As showed in Fig. 4(a), a dependence of J-V characteristics on the doping concentration is observed, indicating the direct charge trapping at the emitter sites of Ir(dmppm)$_2$(dmd). With the increasing of doping concentration from 6% to 10%, the turn-on voltage increased from 3.35 V to 3.40 V, and the current density gradually decreased. We ascribed it to the charge-trapping effect. The HOMO and LUMO levels of TCTA are -5.83 eV and -2.43 eV, respectively,[34] the iridium emitters can be expected as both hole and electron trapping sites because of its deep trap depth of ~ 0.44 eV for holes and ~ 1.0 eV for electrons, it will certainly result the direct formation of excitons on iridium emitters which also avoid the electrical excitation of the widegap host. However, with increasing the doping concentration, the charge carrier transport ability of the emissive layer weakened and consequently lead to increased driving voltages.[35] The decrease in luminance efficiency at higher doping concentrations (*i.e*, 8 and 10 wt.%) is associated with the increased self-quenching of the dopants and the possible triplet-triplet annihilation effect. (Supporting Information).

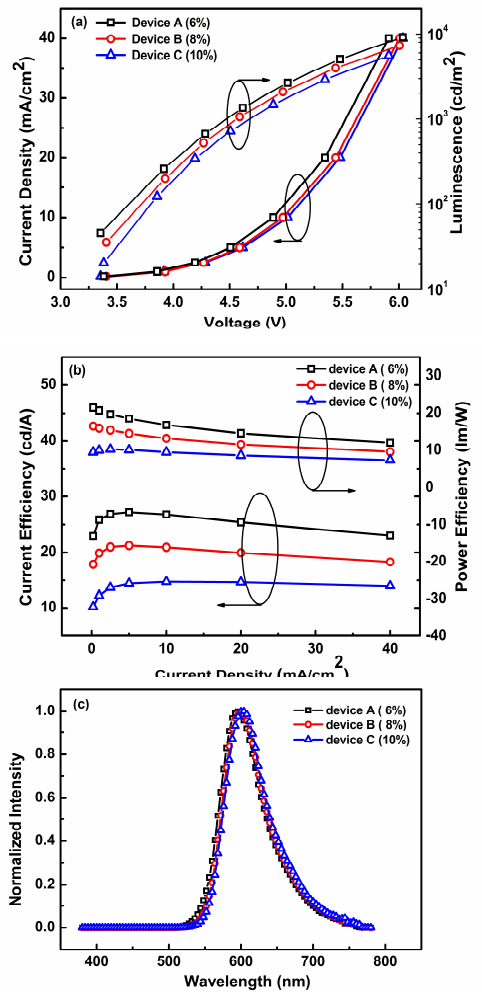

Fig. 4 EL performance of the red device based on Ir(dmppm)$_2$(dmd) with different doping ratios: (a) J-V-L characteristics; (b) LE and PE characteristics; (c) Normalized EL spectra.

The efficiency characteristics of the red devices are shown in Fig. 4(b). In the case of 6 wt.% doping concentration), the device achieved the best performance with a maximum external quantum efficiency of 12%, a luminance efficiency (η_{LE}) of 27.2 cd A^{-1}, and a power efficiency (η_{PE}) of 21.5 lm W^{-1} with saturated red Commission Internationale de l'Eclairage (CIE) coordinates of (0.60, 0.40). Especially, at a high brightness of 5000 cd m^{-2}, the η_{LE} and η_{PE} still remains as 25.4 cd A^{-1} and 14.6 lm W^{-1} with a low roll-off. Fig. 4(c) shows electroluminescence (EL) spectra of TCTA: Ir(dmppm)$_2$(dmd) blend films with various concentrations of 6% 8%, and 10%. Devices A-C exhibit the same red color emission with the changing doping concentrations. And the EL spectra of the devices matched well with their corresponding PL spectra in terms of spectral profile and position in solution, indicating that the EL emission was originated from the triplet excited state of the complex. A slight red-shift by about 4 nm, which is assumed to be the effect of the electrical field on the excited states in OLEDs,[36] was observed in the EL spectra of both devices with different doping concentration in comparison with their PL spectra.

Solution processed white OLEDs

White OLEDs based on three primary colors is an excellent strategy because it is easier to achieve the standard white light with CIE coordinates of (0.33, 0.33).[37,38] However, processing complexity, high operational voltage, and undesired spectral variation are the big issues.[39] To cut down the manufacturing cost, WOLEDs with simple device structure, complementary two-element emissions and solution processing are preferred.[40-41] From the viewpoint of lighting, white OLEDs tend to be designed to emit yellow-white emission, which is thereby considered as physiologically friendly illumination.[42] Herein, we fabricated two-color solution processed WOLEDs with a structure of ITO/PEDOT:PSS (40nm)/TCTA: Firpic: Ir(dmppm)$_2$(dmd) (100: x : 1, 60 nm)/TPBI (45 nm)/Liq (2 nm)/Al (120 nm). (x=20 device D, 30 device E, 40 device F, 50 device G), The EL performance, including J-V-L curves, η_{LE} and EL spectra, are presented in Fig. 5. And the detailed device parameters are summarized in Table 1. Here, the doping ratio of Firpic was fixed at 20 wt% and the blending ratio between Firpic/Ir(dmppm)$_2$(dmd) was tuned to optimize the device performance.

Fig. 5(a) shows the EL spectra of these devices at 10 mA cm^{-2}. Two peaks, a major peak at 476 nm and a small shoulder peak at 500 nm from FIrpic, and one major peak at 600 nm from Ir(dmppm)$_2$(dmd) are observed. With increasing the concentration ratio of Ir(dmppm)$_2$(dmd) relative to FIrpic (i.e., from 1:50 to 1:20), the intensity of the orange emission increases obviously. It suggests that more excitons were transferred from FIrpic to Ir(dmppm)$_2$(dmd). And the CIE co-ordinates fluctuates from (0.32,0.41) to (0.45, 0.42), which is more close to the CIE 1931 chromaticity coordinates approach (0.45, 0.41) for better warm-white standard illumination. In addition, the color stability of these devices are very good owing to the simple device structure with a mixed color emission layer resulting in minimized shift of excitons in the recombination zone.

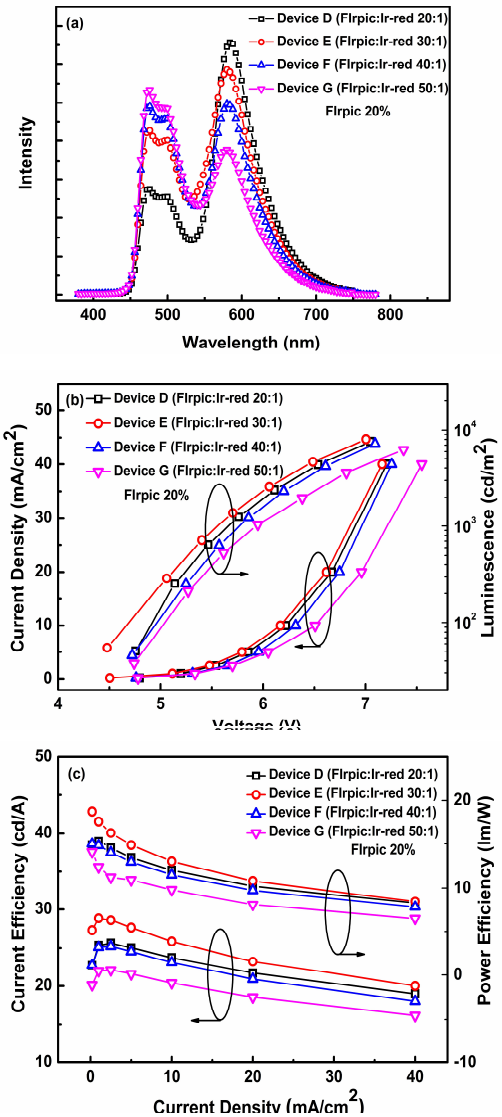

Fig. 5 Device performance of the white device based on different blending ratio between Firpic/Ir(dmppm)$_2$(dmd): (a) EL spectra; (b) J-V-L characteristics; and (c) LE and PE characteristics.

As demonstrated in Fig. 5(b), with gradually increasing the concentration of Ir(dmppm)$_2$(dmd), the driving voltage decreased first and then increased, which is consistent with the change in both the current efficiency and the power efficiency of the device. Fig. 5(c) shows that the best performance was achieved when the blending ratio between Firpic/Ir(dmppm)$_2$(dmd) was 30:1 with an EQE of 12.1% and a LE 28.9 cd A^{-1}, a PE of 18.7 lm W^{-1}. At a high brightness of 5000 cd m^{-2}, the EQE remains at 9.8% with a small roll-off.

Table1 Device performance of red OLEDs A-C and two color WOLEDs D-G.

Device	Doping concentration	$V_{turn-on}$/ (V)	L_{max}/ (cd m^{-2})[c]	η_L/ (cd A^{-1})[c]	η_p/ (lm W^{-1})[c]	EQE (%)[c]	CIE (x,y)[d]
A	6 [a]	3.35	9209	27.2	21.5	12.0	(0.59,0.40)
B	8 [a]	3.38	7303	21.2	16.5	10.1	(0.60,0.40)
C	10 [a]	3.40	5586	14.7	10.2	7.4	(0.60,0.40)
D	20:1 [b]	4.56	7595	25.6	15.3	10.9	(0.45,0.42)
E	30:1 [b]	4.50	8013	28.9	18.7	12.1	(0.39,0.42)
F	40:1 [b]	4.76	7207	25.2	15.0	10.9	(0.36,0.42)
G	50:1 [b]	4.78	6263	22.1	14.1	9.7	(0.32,0.41)

[a] $Ir(dmppm)_2(dmd)$ weight ratio. [b] FIrpic:$Ir(dmppm)_2(dmd)$ weight ratio. [c] Data were collected at Maximum value. [d] CIE were collected at a current density of 10 mA cm^{-2}.

However, the best CIE of the device happened when the blending ratio is 20:1 with an EQE of 10.9% and a LE 25.6 cd A^{-1}, a PE of 15.3 lm W^{-1} respectively. In such two-color white WOLEDs systems, the low driving voltage, low-efficiency roll-off, and higher color qualities can be satisfied with the requirements for illumination applications.

Conclusions

In summary, a solution-processable phosphorescent iridium complex $Ir(dmppm)_2(dmd)$ by using pyrimidine-based ligand was synthesized and successfully applied to fabricate high performance red and white OLEDs. This iridium complex was characterized with orange-red emission at 600 nm corresponding to the CIE coordinates of (0.60, 0.40). The EL efficiency of 27.2 cd A^{-1}, 21.5 lm W^{-1} and EQE of 12% obtained at a doping concentration of 6 wt.% for $Ir(dmppm)_2(dmd)$, which are among the best performance ever reported for partially solution-processed red OLEDs so far. What's more, white OLEDs with a simple device structure were achieved by combining these orange-red phosphors with the traditional blue emitter. A maximum luminance efficiency of 25.6 cd $A^{-1}$and a PE of 15.3 lm W^{-1} with a CIE of (0.45, 0.41) were realized, which is a requirement for a red-dominant warm white light from the physiologically-friendly point of view. With the high efficiency and easy fabrication process, this complex is a promising phosphorescent dopant in solution-processed OLEDs.

Materials and methods

All chemicals i.e., 3,5-dimethylphenylboronic acid, 4,6-dichloropyrimidine and tetrakis(triphenylphosphine)platinum were purchased from Bepharm limited Company. And all of materials used without further purification. THF was purified by PURE SOLV (Innovative Technology) purification system. Chromatographic separations were carried out by using silica gel (200-300 nm). All other reagents were used as received from commercial sources unless otherwise stated. ^1H NMR and ^{13}C NMR spectra were recorded on a Varian Unity Inova 400 spectrometer at room temperature. Mass spectra were recorded on a Thermo ISQ mass spectrometer using a direct exposure probe. UV-Vis absorption spectra were recorded on a Perkin Elmer Lambda 750 spectrophotometer. PL spectra and phosphorescent spectra were recorded on a Hitachi F-4600 fluorescence spectrophotometer. Cyclic voltammetry (CV) was carried out on a CHI600 voltammetric analyzer at room temperature with a conventional three-electrode configuration consisting of a platinum disk working electrode, a platinum wire auxiliary electrode, and an Ag wire pseudo-reference electrode with ferrocenium–ferrocene (Fc^+/Fc) as the internal standard. Nitrogen-purged DCM was used as solvent for the oxidation scan and DMF for the reduction scan with tetrabutylammonium hexafluorophosphate (TBAPF6) (0.1 M) as the supporting electrolyte. The cyclic voltammograms were obtained at a scan rate of 100 mV/s.

Synthesis of $Ir(dmppm)_2(dmd)$

2,4-dichloropyrimidine (4.0 g, 26.8 mmol), 3,5-dimethylphenylboronic acid (8.9 g, 59.1 mmol) and tetrakis(triphenylphosphine)palladium(0) (0.3 g, 2.9 mmol) were dissolved in 50 ml THF/2 M K_2CO_3 (3/1, v/v). The reaction mixture was heated to 60 °C for 8 h under an argon atmosphere. After cooling to room temperature, the organic layer was separated and evaporated to remove solvent. The residue was purified by column chromatography with 1:3 (v/v) dichloromethane/petroleum ether as the eluent and recrystallized from dichloromethane/petroleum to give the ligand 2,4-phenylpyrimidine (5.3g, 86%). Then, $IrCl_3 \cdot nH_2O$ (0.38 g, 1.0 mmol) and the ligand 2,4-phenylpyrimidine (0.51g, 2.2 mmol) were added to a round-bottom flask containing a mixture of 2-ethoxyethanol and water (3:1, v/v, 16 mL). The mixture was then stirred under nitrogen at 120 °C for 24 h and cooled to room temperature. The precipitate that formed was filtered and washed with H_2O, methanol, ether, and n-hexane. The solid was dried in vacuum to give the corresponding cyclometaled dichloride bridged iridium (III) dimers. To a 25 mL flask were added the dimer, K_2CO_3 (0.15 g, 1.1 mmol), acetoacetone (1.1 mmol), and 2-ethoxyethanol

(5 mL). The mixture was stirred at 80 °C under a nitrogen atmosphere for 12 h. After cooling to room temperature, the mixture was filtered and the solid was collected and washed with methanol, ether, and n-hexane to give desired iridium complex $Ir(dmppm)_2(dmd)$ in 42% yield. ^1H NMR (400 MHz, $CDCl_3$) δ (ppm): 8.88 (s, 2H) 8.10 (s, 2H) 7.83-7.73 (m, 5H, J=8.0 Hz,) 7.56 (s, 2H) 6.66 (s, 3H) 5.19 (s, 1H) 2.48-2.16 (m, 24H) 1.61-1.46 (m, 14H). ^{13}C NMR (100 MHz, $CDCl_3$) δ (ppm): 193.2, 175.2, 157.7, 146.6, 145.7, 144.4, 138.6, 136.2, 133.6, 132.6, 130.4, 125.2, 125.0, 109.1, 39.4, 23.8, 21.4, 20.8, 20.2, 19.8. MS (MALDI-TOF): m/z 922.54 [M^+]. Anal. calcd for $C_{37}H_{29}IrN_4O_2$ (%): C 63.82, H 5.79, N 6.08; found: C 63.74, H 5.82, N 6.05.

Device Fabrication and Measurement.

The patterned ITO glass substrates with a sheet resistance of about 20 Ω square^{-1} were pre-cleaned with routine procedure, first by a surfactant scrub, and then beginning with acetone, ethanol, deionized water inside an ultrasonic bath. After a UV-ozone treatment for 20 min, a 40 nm thick layer of PEDOT:PSS was deposited on the ITO substrate via spin-coating to form a hole injection layer and then were baked in oven at 120 °C for 45 min. Afterwards, the samples were moved into a glove box under a nitrogen-protected environment, a 45 nm emissive layer of the mixture of the Ir complex (Firpic) and the host was coated on the top of PEDOT: PSS layer from a chlorobenzene solution with a total concentration of 10 mg mL^{-1} and then annealed at 120 °C for 20 min to remove the solvent residue. And then the sample was transferred to a thermal evaporator chamber (pressure less than 5 ×10^{-4} Pa) , a 40 nm TPBI layer was deposited followed by 2 nm Liq as an electron injection layer and the 120 nm thick aluminium layer as the cathode sequentially. The overlapping area between the cathode and anode defined a pixel size of 9 mm^2.

The Current-luminance-voltage characteristics of the EL devices were measured by a Keithley source measurement unit (Keithley 2400 and Keithley 2000) with a calibrated silicon photodiode. The EL spectra were measured by SpectraScan PR650 spectrophotometer. All measurements were carried out at room temperature under ambient conditions. Ultraviolet photoemission spectroscopy (UPS) analysis was carried out using an unfiltered He I (21.2 eV) gas discharge lamp and a hemispherical analyzer. Atomic force microscopy (AFM) images of the interfacial films were obtained using a Veeco Multimode V instrument.

Acknowledgements

We acknowledge financial support from the Natural Science Foundation of China (Nos. 61307036 and 61177016) and from the Natural Science Foundation of Jiangsu Province (No. BK20130288). This project is also funded by the Collaborative Innovation Center of Suzhou Nano Science and Technology, and by the Priority Academic Program Development of Jiangsu Higher Education Institutions (PAPD).

Notes and references

Jiangsu Key Laboratory for Carbon-Based Functional Materials & Devices, Institute of Functional Nano & Soft Materials (FUNSOM), and Collaborative Innovation Center of Suzhou Nano Science and Technology, Soochow University, Suzhou, Jiangsu 215123, China

Email: lsliao@suda.edu.cn; zkwang@suda.edu.cn

Electronic Supplementary Information (ESI) available: [UPS spectrum of $Ir(dmppm)_2(dmd)$ and the ^1H NMR, ^{13}C NMR spectra of $Ir(dmppm)_2(dmd)$]. See DOI: 10.1039/b000000x/

1 C.W. Tang, S. A. VanSlyke, *Appl. Phys. Lett.*, 1987, 51, 913 -915.
2 L. S. Liao, W. K. Slusarek, T. K. Hatwar, M. L. Ricks, D. L. Comfort, *Adv. Mater.*, 2008, 20, 324-329.
3 S. Kim, H. J. Kwon, S. Lee, H. Shim, Y. Chun, W. Choi, J. Kwack, D. W. Han, M. Song, S. Kim, S. Mohammadi, I. Kee, S. Y. Lee, *Adv. Mater.*, 2011, 23, 3511-3516.
4 S. Reineke, F. Lindner, G. Schwartz, N. Seidler, K. Walzer, K. Leo, *Nature*, 2009, 459, 234-238.
5 H. Sasabe, J. Kido, *Chem. Mater.*, 2010, 23, 621 -630.
6 Q. Zhang, T. Komino, S. Huang, S. Matsunami, K. Goushi, C. Adachi, *Adv. Funct. Mater.*, 2012, 22, 2327 -2336.
7 M. A. Baldo, D. F. O'Brien, Y. You, A. Shoustikov, S. Sibley, M. E. Thompson, S. R. Forrest, *Nature*, 1998, 395, 151-154.
8 C. Adachi , M. A. Baldo , M. E. Thompson, S. R. Forrest, *J. Appl. Phys.*, 2001, 90, 5048-5051.
9 a) W. Y. Wong, C. L. Ho, Coord. *Chem. Rev.*, 2009, 253 1709-1758; b) W. Y. Wong, C. L. Ho, *J. Mater. Chem.*, 2009, 19, 4457-4482; c) G. Zhou, W. Y. Wong, X. Yang, *Chem. Asian J.*, 2011, 6, 1706-1727.
10 J. W. Sun, J. H. Lee , C. K. Moon , K. H. Kim , H. Shin, J. J. Kim, *Adv. Mater.*, 2014, 26, 5684-5688.
11 L. S. Cui, Y. M. Xie, Y. K. Wang, C. Zhong, Y. L. Deng, X.Y. Liu, Z. Q. Jiang, L. S. Liao, *Adv. Mater.*, 2015, 27, 4213-4217.
12 D. R. Lee, B. S. Kim, C. W. Lee, Y. Im, K. S. Yook, S. H. Hwang, J. Y. Lee, *ACS Appl. Mat. Interfaces*, 2015, 7, 9625-9629.
13 Q. S. Zhang, B. Li, S. Huang, H. Nomura, H. Tanaka, C. Adachi, *Nature Photon.*, 2014, 8, 326-332.
14 H. Uoyama, K. Goushi, K. Shizu, H. Nomura, C. Adachi, *Nature*, 2012, 492,234-238.
15 T. Furukawa, H. Nakanotani, M. Inoue, C. Adachi, *Sci. Rep.*, DOI: 10.1038/srep08429.
16 a) G. M. Li, D. X. Zhu, T. Peng,Y. Liu, Y. Wang, M. R. Bryce, *Adv. Funct. Mater.*, 2014, 24, 7420-7426; b) Y. Tao, Q. Wang, L. Ao, C. Zhong, J. Qin, C. Yang, D. Ma, *J. Mater. Chem.*, 2010, 20, 1759-1765.
17 Q. Wang, J. Ding, D. Ma, Y. Cheng, L. Wang, F. Wang, *Adv. Mater.*, 2009, 21, 2397-2401.
18 X. Shi, M. Xu, D. Zhou, Z. K. Wang, L. S. Liao, *Appl. Phys. Lett.*, 2013, 102, 233304.
19 N. Aizawa, Y. J. Pu, T. Chiba, S. Kawata, H. Sasabe, J. Kido, *Adv. Mater.*, 2014, 26, 7543-7546.

20 a) C. Liu, Q. Fu, Y. Zou, C. L. Yang, D. G. Ma, J. G. Qin, *Chem. Mater.*, 2014, 26, 3074-3083. b) L. Li, J. J. Liang, S.Y. Chou, X. D. Zhu, X. F. Niu, Z. B.Yu , Q. B. Pei, *Sci. Rep.*, DOI: 10.1038/srep04307. c) Z. Wang, Y. Lou, S. Naka, H. Okada, *Appl. Phys. Lett.* 2010, 97, 203302.

21 R. Wang, D. Liu, R. Zhang, L. Deng, J. Li, *J. Mater. Chem.*, 2012, 2, 1411-1417.

22 Z. Q. Gao, B. X. Mi, H. L.Tam, K. W. Cheah, C. H. Chen, M. S. Wong, S. T. Lee, C. S. Lee, *Adv. Mater.*, 2008, 20, 774-778.

23 X. J. Liu, S. M. Wang, B. Yao, B. H. Zhang, C. L. Ho, W. Y. Wong, Y. X. Cheng, Z.Y. Xie, *Org. Electron.*, 2015, 21, 1-8.

24 M. R. Zhu, T. L. Ye, X. He, X. S. Cao, C. Zhong, D. G. Ma, J. G. Qin, C. L. Yang, *J. Mater. Chem.*, 2011, 21 , 9326-9331.

25 X.W. Zhang, X. Guo, Y. H. Chen, J. Y. Wang, Z. F. Lei, W. Y. Lai, Q. L. Fan, W. Huang, *J. Lumin.*, 2015, 161, 300-305.

26 J. Liu, J. S. Miao, H. B. Wu, *Luminescence*, 2015, 30, 393-396.

27 L. S. Cui, Y. Liu, X. Y. Liu, Z. Q. Jiang, and L. S. Liao, *ACS Appl. Mat. Interfaces*, 2015, 7, 11007-11014.

28 D. Sun, X. Zhou, J. Liu, X. Sun, H. Li, Z. Ren, D. Ma, M. R. Bryce, S. Yan, *ACS Appl. Mat. Interfaces*, 2015, DOI: 10.1021/am507592s.

29 G. T. Lei, L. D. Wang, L. Duan, J. H. Wang and Y. Qiu, *Synth. Met.*, 2004, 144, 249-252.

30 W. Y. Wong, G. J. Zhou, X. M. Yu, H. S. Kwok, B. Z. Tang, *Adv. Funct. Mater.*, 2006, 16, 838 -846.

31 S. Chen, G. Tan, W. Y. Wong, H. S. Kwok, *Adv. Funct. Mater.*, 2011, 21, 3785-3793.

32 M. K. Nazeeruddin, R. T. Wegh, Z. Zhou, C. Klein, Q. Wang, F. D. Angelis, S. Fantacci, M. Gratzel, *Inorg. Chem.*, 2006, 45, 9245 −9250.

33 Z. Q. Wang, C. Xu, X. M. Dong, Y. P. Zhang, X. Q. Hao, J. F. Gong, M. P. Song, B. M. Ji, *Inorg. Chem. Commun.*, 2011, 14, 316 −319.

34 Y. S. Park, K. H. Kim, J. J. Kim, *Appl. Phys. Lett.*, 2013, 102, 153306.

35 (a) J. Shao, J. Chang, C. Chi, *Org. Biomol. Chem.*, 2012, 10, 7045-7052. (b) M. Belletete, S. Beaupre, J. Bouchard, P. Blondin, M. Leclerc, G. Durocher, *J. Phys. Chem. B*, 2000, 104, 9118-9125. (c) X. Zhan, Z.Tan, B. Domercq, Z. An, X. Zhang, S. Barlow, Y. Li, D. Zhu, B. Kippelen, S. R. Marder, *J. Am. Chem. Soc.*, 2007, 129, 7246-7247.

36 H. Yamamoto, J. Wilkinson, J. P. Long, K. Bussman, J. A. Christodoulides and Z. H. Kafafi, *Nano Lett.*, 2005, 5, 2485-2488.

37 S. Hofmann, M. Furno, B. Lüssem, K. Leo, M. C. Gather, *Phys. Status Solidi A*, 2013, 210, 1467 -1475.

38 K. T. Kamtekar, A. P. Monkman, M. R. Bryce, *Adv. Mater.*, 2010, 22, 572 -582.

39 T. Peng, Y. Yang, H. Bi, Y. Liu, Z. Hou, Y. Wang, T. Peng, Y. Yang, H. Bi, Y. Liu, Z. Hou, Y. Wang, *J. Mater. Chem.*, 2011, 21, 3551-3553.

40 D. M. Sun, X. K. Zhou, J. T. Liu, X. L. Sun, H. H. Li, Z. J. Ren, D. G. Ma, M. R. Bryce, S. Yan, *ACS Appl. Mat. Interfaces*, DOI: 10.1021/am507592s.

41 Y. R. Cho, H. S. Kim, Y. J. Yu, M. C. Suh, *Sci. Rep.*, DOI: 10.1038/srep15903.

42 J. H. Jou, C. Y. Hsieh, J. R. Tseng, S. H. Peng, Y. C. Jou, J. H. Hong, C. H. Lin, *Adv. Funct. Mater.*, 2013, 23, 2750-2757.

Table of Contents Entry

A new red phosphorescent material Ir(dmppm)$_2$(dmd) is synthesized and successfully used to fabricate solution-processed red and white organic light-emitting diodes.

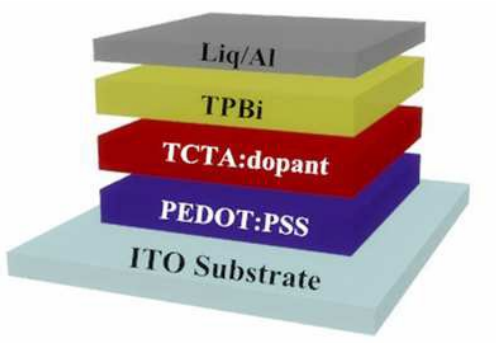

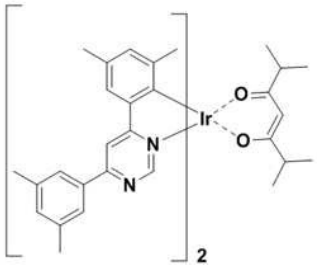

Ir(dmppm)$_2$(tmd)